Photoelectron Spectroscopy of AuO⁻ and AuS⁻

Takatoshi Ichino,* Adam J. Gianola, Django H. Andrews, and W. Carl Lineberger*

JILA and Department of Chemistry and Biochemistry, University of Colorado, Boulder, Colorado 80309

Received: September 16, 2004; In Final Form: October 13, 2004

The 364 nm photoelectron spectra of AuO⁻ and AuS⁻ have been measured. The electron affinities of AuO and AuS have been determined to be 2.374 ± 0.007 and 2.469 ± 0.006 eV, respectively. The electronic ground states of the neutral diatomics are $^2\Pi_i$ states, and the spin–orbit splitting between the $X^2\Pi_{1/2}$ and $^2\Pi_{3/2}$ states is 1440 ± 80 cm⁻¹ for AuO and 1280 ± 60 cm⁻¹ for AuS. A 590 ± 70 cm⁻¹ vibrational peak built off the $^2\Pi_{1/2}$ origin of the AuO spectrum is clearly detected, while the corresponding peak built off the $^2\Pi_{3/2}$ origin is barely detectable. The corresponding 400 ± 30 cm⁻¹ vibration in the AuS spectrum shows the opposite behavior, with the $^2\Pi_{3/2}$ showing the stronger vibrational activity. Franck–Condon analyses of the spectra establish that the equilibrium bond length of $X^1\Sigma^+$AuO⁻ (AuS⁻) differs from the average bond length of the two spin–orbit states of AuO (AuS) by −0.015 ± 0.008 Å (+0.018 ± 0.007 or +0.007 ± 0.007 Å). These bond length relations reflect different extent of relativistic effects between the anions and the neutrals. The intensity of the $X^2\Pi_{1/2}$ origin peak is significantly greater than that of the $X^2\Pi_{3/2}$ origin peak in both AuO and AuS. These features are the results of strong second-order spin–orbit coupling between the $X^1\Sigma^+$ state and $A\,^3\Pi_0$ state in the corresponding anions. The bond length of $X^1\Sigma^+$AuO⁻ has been determined to be 1.899 ± 0.006 Å based upon the bond length of $X^2\Pi_{3/2}$AuO.

Introduction

A considerable time has passed since the discovery of the catalytic activity of gold nanoparticles supported on transition metal oxides.[1,2] The dependence of the catalytic activity on the size of the gold nanoparticle has continued to intrigue scientists, as the surface of bulk gold is known to be quite inactive.[3,4] Particular attention has been paid to catalytic CO oxidation at low temperature.[1,2,5–9] It has been suggested that the charge transfer from the support transition metal oxide to the gold nanoparticle is an important factor in the catalysis.[10]

Gas-phase cluster studies have determined properties of gold nanoparticles that may be relevant in understanding the catalytic processes. Cox et al. studied the reactivity of cationic, neutral, and anionic gold clusters toward small molecules.[11] They found that the anionic clusters reacted with O_2 only when the clusters contained an even number of gold atoms. Ervin and co-workers found the same effect[12] and suggested that the reactivity arises through a charge-transfer involving an unpaired electron in the gold cluster anion and an unpaired electron in O_2. Whetten and co-workers further studied the reactivity of anionic gold clusters[13–15] and showed that, in the presence of O_2 and CO molecules, coadsorption of both molecules onto the cluster anions takes place. They also observed that the coadsorption of O_2 and CO on the anionic gold clusters led to formation of CO_2. This coadsorption has now been observed on the smallest gold cluster, Au_2^-, at 100 K;[16–18] Castleman et al.[19] have recently reported analogous chemistry employing the atomic gold anion, while reactions with the neutral Au atom were studied a long time ago.[20]

To gain insight into this catalytic reactivity, it is important to characterize the bonding between gold clusters and oxygen. While the simplest example of Au and O bonding is found in the diatomic molecules such as AuO and AuO⁻, they have been

rarely studied experimentally,[21–23] and only a few theoretical studies have been reported.[24,25] Understanding the nature of bonding in AuO and AuO⁻ could be useful in interpreting the size-dependent properties of gold clusters with adsorbates. Here, we report the photoelectron spectra of AuO⁻ and an isovalent system, AuS⁻. The electron affinities (EA) of AuO and AuS have been determined. The ground states of the neutral diatomics have been identified as $^2\Pi_i$ states, and their spin–orbit splitting constants have been obtained. The bond lengths of the diatomics are significantly different between the $X^2\Pi_{1/2}$ and $^2\Pi_{3/2}$ states, such that the Franck–Condon overlap in the transition from the anion to the neutral is quite different between the two spin–orbit states. The analysis of the spectra allows us to determine the bond length difference between the anion ground states ($^1\Sigma^+$) and the neutral $X^2\Pi_i$ states. The bond length of $X^1\Sigma^+$AuO⁻ has been derived using the bond length of $X^2\Pi_{3/2}$AuO determined in recent FT-near-IR measurements by O'Brien and co-workers.[26] The results are discussed in relation to the other coinage metal oxides, CuO and AgO. Comparison between gold and other coinage metal oxides reveals the strong relativistic effects in the gold system. The intensities and photoelectron angular distributions show clearly the importance of second-order spin–orbit coupling in the anions.

Experimental Procedures

The photoelectron spectrometer has been described in detail previously,[27] so only a brief description will be given next. The anions, AuO⁻ and AuS⁻, are formed in a simple sputter ion source located in a flowing afterglow ion source operated at 0.5 Torr.[28] Trace amounts of O_2 (CS_2) are introduced downstream in the flow tube to produce AuO⁻ (AuS⁻). The negative ions are thermalized through collisions with the buffer gas, extracted into a low-pressure region, and mass analyzed with a Wien filter. Typical beam currents are ~5 pA. The selected ions are refocused and decelerated into the interaction region, where they cross a 100 W, 363.8 nm laser beam, obtained

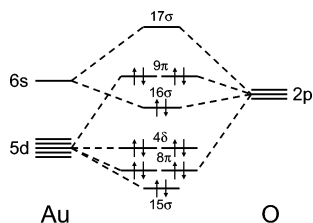**11308** *J. Phys. Chem. A, Vol. 108, No. 51, 2004*

Ichino et al.

Figure 1. Schematic representation of molecular orbitals and electronic configuration of $X^1\Sigma^+$AuO$^-$.

through the use of a high-Q buildup cavity. A small portion of the photodetached electrons are energy analyzed in a hemispherical energy analyzer with a resolution of ~15 meV. The photoelectron spectrum of atomic gold anion is measured to calibrate the electron energy scale (EA(Au) = 2.30863 ± 0.00003 eV).[29,30] The photoelectron angular distributions are obtained by recording spectra as a function of the direction of the electric field polarization of the laser beam, controlled with a rotatable half-wave plate. The angular distribution of photoelectrons can be expressed as[31]

$$I(\theta) = \frac{\sigma_o}{4\pi}(1 + \beta P_2(\cos\theta)) \qquad (1)$$

where σ_0 is the total photodetachment cross section, β is the anisotropy parameter, $P_2(\cos\theta)$ is the second Legendre polynomial, and θ is the angle between the electron collection direction and the laser electric field vector. Photoelectron spectra were measured at $\theta = 0$, 54.7, or 90°, to obtain both the average cross section and the anisotropy parameter.

Calculations

Electronic structure calculations are carried out using the MOLPRO 2002.3 suite of programs.[32] The methods employed are single and double excitation coupled cluster with perturbative triples (CCSD(T))[33-36] and internally contracted multireference configuration interaction with single and double excitations (MRCI).[37,38] Restricted open-shell Hartree−Fock orbitals and unrestricted Hartree−Fock orbitals are used in CCSD(T) and MRCI calculations for open-shell systems, respectively. The orbital space used for correlation calculations in MRCI includes 5d, 6s, and 6p orbitals of Au atom and 2s and 2p orbitals of O atom or 3s and 3p orbitals of S atom. Among the molecular orbitals, the two lowest σ orbitals, the two lowest π orbitals, and the two δ orbitals are constrained to be doubly occupied. All the inner orbitals are optimized at CASSCF calculations and frozen during MRCI calculations. Spin−orbit calculations are carried out using state-averaged CASSCF reference wave functions with spin−orbit pseudopotentials for Au. For AuO$^-$ and AuS$^-$, the $X^1\Sigma$ state, $A^3\Pi$ states (x, y), and $^1\Pi$ states (x, y) are included in the spin−orbit calculations. Small-core, energy-consistent, relativistic pseudopotentials developed by Stuttgart group[39] are used to represent 60 electrons of Au atom. Nonrelativistic pseudopotentials[24] are also used to compare the results with relativistic calculations. Basis sets for the corresponding pseudopotentials are used for Au with augmentation of three f functions (exponents: 1.41, 0.47, and 0.15) as used in the literature.[40] Augmented-cc-pVTZ basis sets are used for O and S atoms.[41-43]

Results

Figure 1 shows a schematic representation of the molecular orbitals of AuO$^-$. The electronic structure calculations[25] predict that the ground state is $^1\Sigma^+$ for both AuO$^-$ and AuS$^-$. In
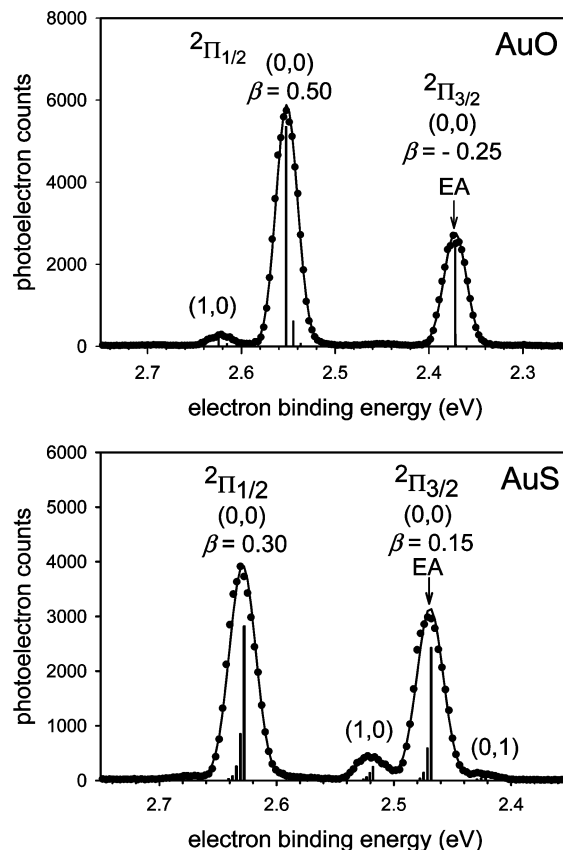
Figure 2. 364 nm photoelectron spectra of (a) AuO$^-$ and (b) AuS$^-$ taken at the magic angle (solid circles). The sticks represent transition energies as well as the relative intensities calculated in the Franck−Condon simulation as described in the text. The solid curves represent the simulated spectra with an fwhm of 25 meV.

$X^1\Sigma^+$AuO$^-$, the electrons fill up to 9π orbitals. Photodetachment of an electron from the HOMO leads to formation of $X^2\Pi_i$-AuO. The negative spin−orbit coupling constant for the ground state is expected, in analogy with CuO and AgO.[44-47] Since formation of the electronically excited states of AuO (such as $^2\Sigma^+$) requires higher photon energy than that used in our experiment (3.408 eV), only the $X^2\Pi_i$ state of AuO is expected to be present in the photoelectron spectrum. The same situation applies for AuS$^-$. While it may be appropriate to use Hund's case (c) notation for the electronic states in these gold systems with the large spin−orbit effects, we, however, chose to use Hund's case (a) notation throughout this paper for the sake of convenience in discussion.

AuO$^-$. The photoelectron spectrum of AuO$^-$ obtained at the magic angle is shown in Figure 2a. There are two relatively intense peaks in the spectrum. The peak at an electron binding energy[48] (eBE) ~2.55 eV is twice as intense as that at eBE ~2.37 eV. The β values are found to be 0.50 and −0.25 for the two peaks at the higher and lower eBE, respectively. These two peaks represent the $X^2\Pi_{1/2}$ and $^2\Pi_{3/2}$ states ($v' = 0$) of AuO, respectively. A $v' = 1$ peak is seen built off the $X^2\Pi_{1/2}$ origin, while no such peak is observed in the $X^2\Pi_{3/2}$ portion.

A Franck−Condon analysis was performed for the two spin−orbit states independently, using the PESCAL program.[49] The program allows us to calculate the Franck−Condon factors, based on Morse oscillators for the anion and neutral states, by numerically integrating the products of Laguerre wave function. Parameters in the calculations include the vibrational frequencies, difference in bond lengths of the anion and neutral states, and the vibrational temperature of the anion. On the basis

TABLE 1: Molecular Parameter Values Determined through the Franck–Condon Fitting of the Photoelectron Spectra of AuO⁻ and AuS⁻ and Results of CCSD(T) Calculations

	AuO⁻($X^1\Sigma^+$)	AuO($X^2\Pi_{3/2}$)	AuO($X^2\Pi_{1/2}$)
T_e	−2.374 (7) eV	0	1440 (80) cm⁻¹
r_e (Å)	1.899 (6)[a]	1.912[b]	1.917 (10)[a]
ω_e (cm⁻¹)	c		590 (70)
T_e CCSD(T)[d]	−2.26 eV		
r_e (Å), CCSD(T)	1.888		1.907[e]

	AuS⁻($X^1\Sigma^+$)	AuS($X^2\Pi_{3/2}$)	AuS($X^2\Pi_{1/2}$)
T_e	−2.469 (6) eV	0	1280 (60) cm⁻¹
r_e (Å)	R	R − 0.025 (7)	R ± 0.011 (6)
ω_e (cm⁻¹)	380 (60)	400 (30)	
T_e, CCSD(T)[d]	−2.43 eV		
r_e (Å), CCSD(T)	2.233		2.219[e]

[a] The most likely value; see the text. [b] Determined by O'Brien et al. (the accompanying paper, ref 26). [c] A vibrational frequency of 650 cm⁻¹ was assumed in the fitting. [d] Zero-point energy correction is neglected. [e] Average of the two spin–orbit substates.

of the χ^2 evaluation in the fitting procedure, those parameters are optimized as well as the peak positions from which the electron affinity and the spin–orbit splitting constant have been determined. The error bars for the optimized parameters represent a 95% confidence level.

The optimized fitting is shown as a solid line in Figure 2a, and the optimized parameters are given in Table 1. Because there is no apparent hot band in the spectrum, the vibrational temperature of AuO⁻ was assumed to be the same as that of AuS⁻, 450 K. A vibrational frequency of AuO⁻ was assumed as given in Table 1. By fitting the $X^2\Pi_{3/2}$ portion of the spectrum, the EA of AuO is found to be 2.374 ± 0.007 eV. Table 1 also shows that the CCSD(T) calculations predict the EA to be 2.26 eV, in good agreement with this experimental value. The equilibrium bond length relation between $X^1\Sigma^+$AuO⁻ and $X^2\Pi_{3/2}$AuO is $r_e(X^1\Sigma^+) = r_e(X^2\Pi_{3/2}) ± (0.013 ± 0.006)$ Å. The sign of the bond length difference cannot be determined definitively from the Franck–Condon fitting. Recently, O'Brien measured AuO emission spectrum and determined $r_e(X^2\Pi_{3/2})$ = 1.912 Å.[26] With this value, the anion bond length becomes $r_e(X^1\Sigma^+) = 1.899 ± 0.006$ or $1.925 ± 0.006$ Å. By fitting the $X^2\Pi_{1/2}$ portion of the spectrum, the spin–orbit splitting of the $X^2\Pi_i$ states has been found to be −1440 ± 80 cm⁻¹. On the basis of the atomic orbital composition of the AuO π orbital, O'Brien estimated the spin–orbit splitting to be about −1000 cm⁻¹,[26] which is consistent with our experimental finding. The bond length relation between $X^1\Sigma^+$AuO⁻ and $X^2\Pi_{1/2}$AuO is $r_e(X^2\Pi_{1/2}) = r_e(X^1\Sigma^+) + (0.018 ± 0.008)$ Å. The sign of the bond length shift is definitive in this case, as explained in the Discussion. Thus, $r_e(X^2\Pi_{1/2}) = 1.917 ± 0.010$ or $1.943 ± 0.010$ Å, depending on which of the two possible bond lengths for $X^1\Sigma^+$AuO⁻ is used. The vibrational frequency is 590 ± 70 cm⁻¹ for $X^2\Pi_{1/2}$AuO. The (1, 0) band for $X^2\Pi_{3/2}$AuO is too weak to determine its vibrational frequency.

AuS⁻. The photoelectron spectrum of AuS⁻ obtained at the magic angle is shown in Figure 2b. Similar to the AuO⁻ spectrum, there are two relatively intense peaks in the spectrum. The peak at the lower eBE, ∼2.47 eV, represents the $X^2\Pi_{3/2}$ state ($v' = 0$), and the other peak at ∼2.63 eV, somewhat more intense than the former, represents the $X^2\Pi_{1/2}$ state ($v' = 0$) of AuS. The photoelectron angular distribution measurements reveal that β is 0.15 for the $X^2\Pi_{3/2}$ origin peak and 0.30 for the $X^2\Pi_{1/2}$ origin peak. The $X^2\Pi_{3/2}$ origin peak is accompanied by a small peak on the higher eBE side and a shoulder on the lower

eBE side, which represent vibrational bands of $X^2\Pi_{3/2}$AuS and $X^1\Sigma^+$AuS⁻, respectively. These satellite bands are not apparent for the $X^2\Pi_{1/2}$ origin peak.

A Franck–Condon analysis was carried out for the AuS⁻ spectrum. The solid line in Figure 2b shows the optimized fitting, and Table 1 provides the optimized parameters. From the fitting of the $X^2\Pi_{3/2}$ portion of the spectrum, the EA of AuS has been determined to be 2.469 ± 0.006 eV. This EA is in good agreement with the value, 2.44 ± 0.03 eV, measured in a time-of-flight photoelectron spectroscopic study.[50] The CCSD-(T) calculations predict the EA to be 2.43 eV (Table 1), consistent with our experimental finding. The $X^2\Pi_{3/2}$AuS vibrational frequency is 400 ± 30 cm⁻¹, while the $X^1\Sigma^+$AuS⁻ vibrational frequency is 380 ± 60 cm⁻¹. The vibrational temperature of AuS⁻ has been found to be about 450 K. The equilibrium bond length relation between $X^1\Sigma^+$AuS⁻ and $X^2\Pi_{3/2}$AuS is $r_e(X^1\Sigma^+) = r_e(X^2\Pi_{3/2}) + (0.025 ± 0.007)$ Å. Fitting of the $X^2\Pi_{1/2}$ peak allows us to determine the spin–orbit splitting between the $X^2\Pi_i$ states to be −1280 ± 60 cm⁻¹ (−0.159 ± 0.007 eV). This number is in fair agreement with that reported by Kaya,[50] −0.18 ± 0.02 eV. The bond length relation between $X^1\Sigma^+$AuS⁻ and $X^2\Pi_{1/2}$AuS is $r_e(X^1\Sigma^+) = r_e(X^2\Pi_{1/2}) ± (0.011 ± 0.006)$ Å. As a result, the bond length relationship between the two spin–orbit states becomes $r_e(X^2\Pi_{1/2}) - r_e(X^2\Pi_{3/2}) = 0.014 ± 0.010$ or $0.036 ± 0.010$ Å, depending on the sign of the bond length shift for the $X^2\Pi_{1/2}$ state.

Discussion

Franck–Condon Analysis. The photoelectron spectra of AuO⁻ and AuS⁻ clearly demonstrate differences in Franck–Condon overlap between the $X^2\Pi_i$ states of the neutral. This difference signifies that the equilibrium bond lengths of the two spin–orbit states are significantly different from each other. Similar observations have been made in the photoelectron spectra of the halogen oxide anions.[51] The ground states of the neutral halogen oxides are $^2\Pi_i$, as in the coinage metal oxides. The vibrational progression is more extensive for the $X^2\Pi_{1/2}$ state than for the $X^2\Pi_{3/2}$ state in the photoelectron spectrum of FO⁻. On the other hand, the $X^2\Pi_{3/2}$ state has the longer vibrational progression for BrO and IO. The ground states of halogen oxide anions have considerably greater bond lengths than the corresponding neutrals. Therefore, the Franck–Condon profiles observed in the spectra indicate that the bond length of the $X^2\Pi_{1/2}$ state is shorter than that of the $X^2\Pi_{3/2}$ state for FO, while the opposite applies for BrO and IO.

These bond length differences between the $X^2\Pi_i$ states of halogen oxides can be understood with a well-known expression for the effective rotational constants of the two spin–orbit states (up to second-order),[52]

$$B_{\mathrm{eff}} = B ± \left[\frac{A_{\mathrm{D}}}{2} + \frac{(B - \gamma/2)^2}{A - 2B}\right] \qquad (2)$$

where B is the unperturbed rotational constant, A is the spin–orbit coupling constant, γ is the constant for spin-rotation interaction, and A_{D} is the constant for centrifugal distortion of spin–orbit coupling. The positive sign corresponds to the $^2\Pi_{3/2}$ state and the negative sign to the $^2\Pi_{1/2}$ state. For the $X^2\Pi_i$ states of halogen oxides, $A < 0$ and $A_{\mathrm{D}} > 0$;[51–61] the two terms inside the bracket in eq 2 have opposite senses. The FO $X^2\Pi_i$ states have a relatively large B and a relatively small magnitude of A and A_{D}.[54,56,58,60] Thus, the second term inside the bracket is dominant over the first term, and B_{eff} is larger for the $X^2\Pi_{1/2}$ state than the $X^2\Pi_{3/2}$ state of FO. Meanwhile, the magnitude of

A_D is quite large for BrO and IO,[52,53,59,60] and the $X^2\Pi_{3/2}$ state has a larger B_{eff} than the $X^2\Pi_{1/2}$ state in these systems. These relations of B_{eff} between the $X^2\Pi_i$ states of halogen oxides are consistent with the difference in Franck−Condon factors observed in the photoelectron spectra.[51]

As there have been no gas-phase spectroscopic studies other than O'Brien's FT-near-IR measurements,[26] A_D is unknown for AuO and AuS. For CuO, AgO, and CuS, it has been experimentally found that $A_D > 0$, and B_{eff} $(X^2\Pi_{1/2})$ $<$ B_{eff} $(X^2\Pi_{3/2})$.[44−47,62−64] Observing the trend in the halogen oxide series, it is certain that $A_D > 0$ for AuO and AuS, and their magnitude is larger than the corresponding Cu or Ag chalcogenides. Thus, B_{eff} $(X^2\Pi_{1/2})$ $<$ B_{eff} $(X^2\Pi_{3/2})$ for AuO and AuS as well; that is, $r_e(X^2\Pi_{1/2}) > r_e(X^2\Pi_{3/2})$. With this bond length relation between the two spin−orbit states, the photoelectron spectra of AuO$^-$ and AuS$^-$ immediately lead us to conclude that $r_e(X^1\Sigma^+)$ is shorter than the average of $r_e(X^2\Pi_{1/2})$ and $r_e(X^2\Pi_{3/2})$ in the oxide and longer in the sulfide system. Consequently, $r_e(X^1\Sigma^+) < r_e(X^2\Pi_{1/2})$ for the oxide and $r_e(X^1\Sigma^+) > r_e(X^2\Pi_{3/2})$ for the sulfide. However, from our measurements alone, it is impossible to determine the analogous bond length relations between the anion and the other spin−orbit state of the neutral.

Table 1 gives the equilibrium bond lengths optimized with CCSD(T) calculations. The CCSD(T) calculations predict $r_e(X^1\Sigma^+) = 1.888$ Å for AuO$^-$ and $r_e(X^2\Pi) = 1.907$ Å for AuO. These results agree with our experimental finding that $r_e(X^1\Sigma^+)$ is shorter than the average of $r_e(X^2\Pi_{1/2})$ and $r_e(X^2\Pi_{3/2})$. Seminario et al. predict $r_e(X^1\Sigma^+) = 1.910$ Å and $r_e(X^2\Pi) = 1.925$ Å with DFT calculations,[25] while DFT results by Kimble et al. give $r_e(X^1\Sigma^+) = 1.882$ Å.[19] We also performed MRCI calculations, and the results are $r_e(X^1\Sigma^+) = 1.895$ Å and $r_e(X^2\Pi) = 1.907$ Å for the oxide system. Considering these electronic structure calculations, $r_e(X^1\Sigma^+) = 1.899 \pm 0.006$ Å is the more likely value of the two possible bond lengths determined in our experiment. With this anion bond length, $r_e(X^2\Pi_{1/2})$ $-$ $r_e(X^2\Pi_{3/2}) = 0.005$ (+0.010, −0.005) Å. If the other anion bond length were adopted, then $r_e(X^2\Pi_{1/2})$ $-$ $r_e(X^2\Pi_{3/2})$ would be 0.031 ± 0.010 Å. For comparison, a rotational spectroscopic study has revealed that the bond length relation between the IO $X^2\Pi_i$ states is $r_e(X^2\Pi_{1/2})$ $-$ $r_e(X^2\Pi_{3/2})$ $= 0.01706$ Å.[52]

CCSD(T) calculations show $r_e(X^1\Sigma^+) = 2.233$ Å for AuS$^-$ and $r_e(X^2\Pi) = 2.219$ Å for AuS (Table 1). Thus, CCSD(T) calculations predict a longer bond length for the anion ground state than the neutral, opposite of the bond length relation for the oxide. This prediction is in accord with our experimental finding. DFT calculations also find a longer bond length in the anion than the neutral, $r_e(X^1\Sigma^+) = 2.260$ Å and $r_e(X^2\Pi) = 2.240$ Å.[25]

Relativistic Effects of Au. It is well-known that Au exhibits substantial relativistic effects.[65−67] The relativistic effects of Au become apparent when compared with Cu and Ag systems. The EA of AuO (2.374 ± 0.007 eV), for instance, is much larger than those of CuO and AgO; EA (CuO) $= 1.777 \pm 0.006$ eV[68] and EA (AgO) $= 1.654 \pm 0.002$ eV.[69] This difference reflects the difference in the atomic electron affinity;[29,30] EA (Cu) $= 1.23579 \pm 0.00004$ eV, EA (Ag) $= 1.30447 \pm 0.00002$ eV, and EA (Au) $= 2.30863 \pm 0.00003$ eV. The larger electron affinity of Au atom originates from the relativistic contraction of Au 6s orbital.[65−67] Another manifestation of relativistic effects is the equilibrium bond length of AuO, $r_e(X^2\Pi_{3/2}) = 1.912$ Å, which is much shorter than that of AgO, as discussed by O'Brien.[26]
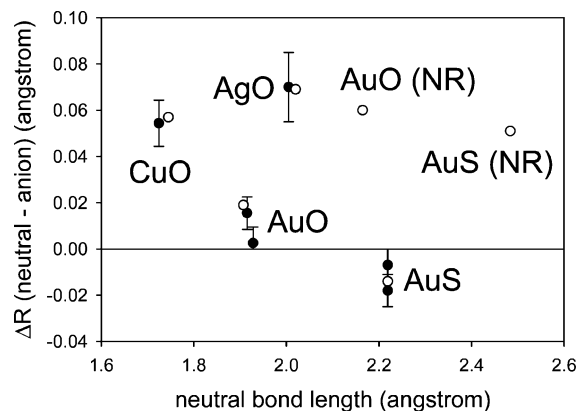

Figure 3. Plots of the neutral−anion bond length difference vs the neutral bond length for the ground states of the coinage metal oxides and sulfide. The solid points are experimental values (see refs 68 and 69), and the open points are values obtained from CCSD(T) calculations for the corresponding ground states. There are two possible experimental values for AuO and AuS (see the text). Also, note that there is no experimental value for the bond length of $X^2\Pi_i$AuS, so the bond length obtained in the CCSD(T) calculations is used to locate the experimental point for AuS. NR stands for nonrelativistic calculations. See the text for details.

Another aspect of Au relativistic effects can be noticed in the difference in the bond length between $X^2\Pi_i$AuO and $X^1\Sigma^+$AuO$^-$, when compared to the Cu and Ag systems. Figure 3 illustrates the equilibrium bond lengths of the $X^2\Pi_i$ states of coinage metal oxides in one dimension, and the bond length difference between the $X^2\Pi_i$ states and the $X^1\Sigma^+$ states of the corresponding anions in the other (solid circles).[68,69] The aforementioned relativistic bond contraction of $X^2\Pi_i$AuO is evident along the neutral bond length coordinate. On the other hand, Figure 3 also shows, in the other coordinate, that the bond length difference between AuO and AuO$^-$ is significantly smaller than that in the Cu and Ag systems. The open circles in Figure 3 represent the results of CCSD(T) calculations performed with relativistic pseudopotentials for all the metal oxides and with nonrelativistic pseudopotentials for the gold oxide. It is evident that the calculations with relativistic pseudopotentials reproduce the experimental results very well. However, nonrelativistic calculations show, in addition to the relativistic bond contraction effect in $X^2\Pi_i$AuO, that the bond length difference between AuO and AuO$^-$ would be comparable to those of the Cu and Ag systems in the absence of relativistic effects.

One possible reason for the small bond length change between AuO and AuO$^-$ would be change in the HOMO character due to the relativistic effect. Bauschlicher and co-workers have studied the electronic structure of CuO and CuS as well as AgO and AgS.[70,71] Their calculations demonstrate significant backdonation from O 2p orbitals to Cu 4p or Ag 5p orbitals in the highest occupied π molecular orbital of the oxides. This interaction renders the π orbital bonding, as found in the photoelectron spectroscopic studies (Figure 3).[68,69] If the bonding character of the π orbital of the gold oxide were significantly less than that of the copper and silver oxides, then it could explain the observed small bond length change between AuO and AuO$^-$. However, when we performed Mulliken population analysis for $X^1\Sigma^+$ CuO$^-$, AgO$^-$, and AuO$^-$ in the relavitistic calculations, we found similar extent of electron back-donation from O 2p orbitals to metal p orbitals for all the anions. Thus, the bonding character of the π orbital is expected to be comparable for all the metal oxide anions.

A more plausible reason would be larger Pauli repulsion effect against the relativistic bond contraction in the anion than in the

neutral. Pauli repulsion has been often considered in the discussion of bonding of metal oxides.[72,73] As one electron is attached to $X^2\Pi_i$AuO to form $X^1\Sigma^+$AuO⁻, the bond attempts to shorten according to the bonding character of the π molecular orbital. However, in the presence of the large relativistic bond contraction $X^2\Pi_i$AuO is already subject to, further bond shortening would face stronger resistance from Pauli orthogonalization repulsion than in the case of nonrelativistic systems, such that it would cancel to some extent the effect of the bonding nature of the π orbital.

The situation is quite the same for AuS⁻. Nonrelativistic calculations show that the bond length increases by 0.051 Å as an electron is detached from $X^1\Sigma^+$AuS⁻ to form $X^2\Pi_i$AuS, while relativistic calculations predict it decreases by 0.014 Å, in agreement with our experimental results (Figure 3). The bond shortening does not mean that the π orbital from which an electron is detached has antibonding character. It is a manifestation of different extent of relativistic bond contraction between the anion and the neutral ground states.

Second-Order Spin−Orbit Coupling Effects. Figure 2a shows that the $X^2\Pi_{1/2}$ origin peak is more intense than the $X^2\Pi_{3/2}$ origin peak of AuO. A similar observation is made in the AuS⁻ spectrum (Figure 2b), even though the intensity disparity is not as great as in the AuO⁻ spectrum. Statistically, the intensity of the two spin−orbit states would be equal, as found in the photoelectron spectra of CuO⁻ and AgO⁻.[68,69] However, deviation from 1:1 intensity ratio is not uncommon. One example is photodetachment from OH⁻ to form $X^2\Pi_i$OH, where rotational spin-uncoupling is quite effective in the Hamiltonian.[74,75] In the heavy diatomics such as AuO or AuS, this rotational effect is not important. Another example is found in the photoelectron spectra of BrO⁻ and IO⁻, where the $X^2\Pi_{3/2}$ vibronic peaks are more intense than the corresponding $X^2\Pi_{1/2}$ vibronic peaks.[51] This intensity difference must arise from the energy dependence of the photodetachment cross section.[76] In the kinetic energy range of about 1 eV or less, the photodetachment cross-section of the HOMO of the halogen oxide anions increases with the kinetic energy of photoelectrons.[77] Thus, the large spin−orbit splitting in BrO or IO results in large difference in the cross section for electron detachment with fixed energy photons between the two spin−orbit states, such that the $X^2\Pi_{3/2}$ peaks appear more intense. It is quite likely that the kinetic energy dependence of the cross-section affects the relative intensity between the two spin−orbit states of AuO and AuS. However, to explain more intense $X^2\Pi_{1/2}$ origin peaks for AuO and AuS, the cross section must be decreasing in the kinetic energy range. It is very hard to conceive such energy dependence in this kinetic energy range, and it is unlikely that the observed intensity disparity originates from such an effect.

The only plausible reason for the unequal intensity of the $X^2\Pi_i$ peaks of AuO and AuS is the second-order spin−orbit coupling effects.[78] As Figure 1 shows, $X^1\Sigma^+$AuO⁻ have electrons filling all the molecular orbitals up to the 9π orbitals. The lowest excited state is $^3\Pi$ where one electron is lifted from the 9π orbital to the 17σ orbital with its spin reversed. Recently, Kimble et al. carried out DFT calculations and found that the A $^3\Pi$ state lies 0.23 eV above $X^1\Sigma^+$AuO⁻ in energy.[19] Considering the energetic proximity and the large spin−orbit coupling constant of Au, it is certain that these two states experience strong second-order spin−orbit coupling, as in the isoelectronic system, HgO.[79] As a result, the ground state of AuO⁻ has significant amount of $^3\Pi$ character. Therefore, there are two possible photodetachment processes for the AuO⁻ ground state

that could lead to formation of $X^2\Pi_i$AuO. One is that an electron is detached from one of the 9π orbitals of the $^1\Sigma^+$ electronic configuration, and the other is that an electron is detached from the 17σ orbital of the $^3\Pi$ configuration. Here, it is important to note that only the $^3\Pi_0$ state, not the $^3\Pi_1$ or $^3\Pi_2$ states, can be mixed with the $X^1\Sigma^+$ state due to the spin−orbit coupling selection rule.[79] This selection rule means that photodetachment from the 17σ orbital of the $^3\Pi_0$ configuration leads to formation of only the $X^2\Pi_{1/2}$ state, not the $X^2\Pi_{3/2}$ state. If the spin−orbit mixing is substantial and the detachment from the 17σ orbital has large cross-section as compared to that from the 9π orbital, then the $X^2\Pi_{1/2}$ peak will appear more intense than the $X^2\Pi_{3/2}$ peak, as observed in our measurements.

Crude quantitative considerations support this idea. The 9π orbitals are mainly O 2p orbitals. The 2p electron photodetachment cross section of O⁻ (^{2}P) to form O (^{3}P) is about 6×10^{-18} cm² at an outgoing electron kinetic energy of 1 eV.[80] On the other hand, the 17σ orbital contains a large contribution from Au 6s orbital (Figure 1). The 6s electron photodetachment cross-section of Au⁻(^{1}S) to form Au(^{2}S) is $(2.6 \pm 0.8) \times 10^{-18}$ cm² at a kinetic energy of about 0.06 eV.[81] This cross-section is expected to become much larger as the kinetic energy approaches ~1 eV. For comparison, the 5s electron photodetachment cross-section of Ag⁻(^{1}S) to form Ag(^{2}S) is $(6.5 \pm 1.0) \times 10^{-17}$ cm² at a kinetic energy of about 0.8 eV.[81] Therefore, it is good to assume the ratio of the cross sections for the 17σ and 9π electron detachment to be 10:1 under our experimental condition. Also, we performed spin−orbit coupling calculations at the MRCI level of theory. The spin−orbit Hamiltonian included the $^1\Sigma^+$, $^3\Pi$ (x, y), and $^1\Pi$ (x, y) states of AuO⁻. Our ab initio spin−orbit calculations show that, at the equilibrium bond length of $X^1\Sigma^+$AuO⁻, the second-order spin−orbit coupling between the $X^1\Sigma^+$ and the $A^3\Pi_0$ states pushes down the $X^1\Sigma^+$ state by 350 cm⁻¹. This result indicates that the proportion of the $^3\Pi_0$ configuration mixed into the ground state through the spin−orbit coupling is about 7%. Thus, based on our ab initio calculations and the aforementioned relative cross sections, the intensity ratio between the $X^2\Pi_{1/2}$ and $^2\Pi_{3/2}$ peaks can be estimated to be $(0.93 + 0.07 \times 10):1 = 1.6:1$ for AuO. The observed origin peak intensity ratio between the two spin−orbit states is roughly 2:1. Thus, this explanation for the relative intensity of the two spin−orbit states is reasonable.[82] The relative intensity of the AuS $X^2\Pi_i$ peaks can be explained in the same way.

Indeed, this second-order spin−orbit coupling effect can be confirmed by observation of different angular distribution between the two spin−orbit states. The β values of the $X^2\Pi_{1/2}$ and the $X^2\Pi_{3/2}$ origin peaks are 0.50 and −0.25, respectively, for AuO, and 0.30 and 0.15, respectively, for AuS. The difference in the β values between the two spin−orbit states is considerable, and it is clear that the kinetic energy dependence of β cannot cause such disparity. In the presence of the second-order spin−orbit coupling, the $X^2\Pi_{1/2}$ peak contains contribution of the 17σ electron detachment. Since the Au 6s orbital plays a major role in the detachment from the 17σ orbital, its anisotropy parameter must be close to 2. Thus, the second-order spin−orbit coupling effect turns β of the $X^2\Pi_{1/2}$ peak more positive than that of the $X^2\Pi_{3/2}$ peak.

Thermodynamics. In the photoelectron spectroscopic studies of CuO⁻ and AgO⁻, the EA of the corresponding neutral radical as well as that of O atom has been used to derive an energetic relation between the bond dissociation energies of the anion and the neutral.[68,69] Similarly, in the present study, the following relations will hold:

$$D_0(Au^- - O) - D_0(Au-O) = EA(AuO) - EA(Au) =$$
$$0.065 \pm 0.007 \text{ eV} \quad (3)$$

$$D_0(Au^- - S) - D_0(Au-S) = EA(AuS) - EA(Au) =$$
$$0.160 \pm 0.006 \text{ eV} \quad (4)$$

Here, D_0 is the bond dissociation energy at 0 K, and EA is the electron affinity. In each case, electron addition to the neutral strengthens the bond by a few kcal mol^{-1}. If the bond dissociation energy of either AuO (AuS) or AuO$^-$ (AuS$^-$) is known, then the other can be derived. Although there have been several experimental studies for AuO,[21,23] no reliable measurements of either of the bond dissociation energies have yet been reported.

Conclusions

The 364 nm photoelectron spectra of AuO$^-$ and AuS$^-$ have been measured, and the Franck−Condon envelops have been analyzed. The electron affinities of AuO and AuS have been determined to be 2.374 ± 0.007 and 2.469 ± 0.006 eV, respectively. The spin−orbit splitting has been found to be −1440 ± 80 cm^{-1} for $X^2\Pi_i$AuO and −1280 ± 60 cm^{-1} for $X^2\Pi_i$AuS. Vibrational frequencies of 590 ± 70 and 400 ± 30 cm^{-1} have been found for $X^2\Pi_{1/2}$AuO and $X^2\Pi_{3/2}$AuS, respectively. Also, a vibrational frequency of 380 ± 60 cm^{-1} has been found for $X^1\Sigma$AuS$^-$. Different Franck−Condon profiles between the two spin−orbit states indicate that the bond length of $X^1\Sigma^+$AuO$^-$ is shorter than the average bond length of $X^2\Pi_i$-AuO, while that of $X^1\Sigma^+$AuS$^-$ is longer than the average bond length of $X^2\Pi_i$AuS. The bond length relation between the anion and neutral ground states reflects considerable relativistic effects. The equilibrium bond length of $X^1\Sigma^+$AuO$^-$ has been determined using the equilibrium bond length of $X^2\Pi_{3/2}$ AuO recently measured by O'Brien.[26] The intensity of the $X^2\Pi_{1/2}$ origin peak is significantly larger than that of the $X^2\Pi_{3/2}$ origin peak in both AuO and AuS. Also, the β value for the $X^2\Pi_{1/2}$ origin peak is more positive than that for the $X^2\Pi_{3/2}$ origin peak in both systems. These results reflect strong second-order spin−orbit coupling between the $X^1\Sigma_0^+$ and $A^3\Pi_0$ states in the anions.

References and Notes

(1) Haruta, M.; Yamada, N.; Kobayashi, T.; Iijima, S. *J. Catal.* **1989**, *115*, 301.
(2) Haruta, M. *Catal. Today* **1997**, *36*, 153.
(3) Hammer, B.; Norskov, J. K. *Nature* **1995**, *376*, 238.
(4) Saliba, N.; Parker, D. H.; Koel, B. E. *Surf. Sci.* **1998**, *410*, 270.
(5) Valden, M.; Lai, X.; Goodman, D. W. *Science* **1998**, *281*, 1647.
(6) Grunwaldt, J. D.; Maciejewski, M.; Becker, O. S.; Fabrizioli, P.; Baiker, A. *J. Catal.* **1999**, *186*, 458.
(7) Grunwaldt, J. D.; Baiker, A. *J. Phys. Chem. B* **1999**, *103*, 1002.
(8) Lopez, N.; Norskov, J. K. *J. Am. Chem. Soc.* **2002**, *124*, 11262.
(9) Liu, Z. P.; Hu, P.; Alavi, A. *J. Am. Chem. Soc.* **2002**, *124*, 14770.
(10) Sanchez, A.; Abbet, S.; Heiz, U.; Schneider, W. D.; Hakkinen, H.; Barnett, R. N.; Landman, U. *J. Phys. Chem. A* **1999**, *103*, 9573.
(11) Cox, D. M.; Brickman, R.; Creegan, K.; Kaldor, A. *Z. Phys. D: At., Mol. Clusters* **1991**, *19*, 353.
(12) Lee, T. H.; Ervin, K. M. *J. Phys. Chem.* **1994**, *98*, 10023.
(13) Salisbury, B. E.; Wallace, W. T.; Whetten, R. L. *Chem. Phys.* **2000**, *262*, 131.
(14) Wallace, W. T.; Whetten, R. L. *J. Phys. Chem. B* **2000**, *104*, 10964.
(15) Wallace, W. T.; Whetten, R. L. *J. Am. Chem. Soc.* **2002**, *124*, 7499.
(16) Hakkinen, H.; Landman, U. *J. Am. Chem. Soc.* **2001**, *123*, 9704.
(17) Hagen, J.; Socaciu, L. D.; Elijazyfer, M.; Heiz, U.; Bernhardt, T. M.; Woeste, L. *Phys. Chem. Chem. Phys.* **2002**, *4*, 1707.
(18) Socaciu, L. D.; Hagen, J.; Bernhardt, T. M.; Woeste, L.; Heiz, U.; Hakkinen, H.; Landman, U. *J. Am. Chem. Soc.* **2003**, *125*, 10437.
(19) Kimble, M. L.; Castleman, A. W.; Mitric, R.; Burgel, C.; Bonacic-Koutecky, V. *J. Am. Chem. Soc.* **2004**, *126*, 2526.
(20) Huber, H.; McIntosh, D.; Ozin, G. A. *Inorg. Chem.* **1977**, *16*, 975.
(21) Smoes, S.; Vanderau, A.; Drowart, J.; Mandy, F. *Bull. Soc. Chim. Belg.* **1972**, *81*, 45.
(22) Griffiths, M. J.; Barrow, R. F. *J. Chem. Soc., Faraday Trans.* **1977**, *73*, 943.
(23) Hecq, A.; Vandy, M.; Hecq, M. *J. Chem. Phys.* **1980**, *72*, 2876.
(24) Schwerdtfeger, P.; Dolg, M.; Schwarz, W. H. E.; Bowmaker, G. A.; Boyd, P. D. W. *J. Chem. Phys.* **1989**, *91*, 1762.
(25) Seminario, J. M.; Zacarias, A. G.; Tour, J. M. *J. Am. Chem. Soc.* **1999**, *121*, 411.
(26) O'Brien, L. C.; Hardimon, S. C.; O'Brien, J. J. *J. Phys. Chem. A* **2004**, *108*, 11302.
(27) Ervin, K. M.; Lineberger, W. C. Photoelectron Spectroscopy of Negative Ions. In *Advances in Gas-Phase Ion Chemistry*; Adams, N. G., Babcock, L. M., Eds.; JAI Press: Greenwich, 1992; Vol. 1; p 121.
(28) Ho, J.; Ervin, K. M.; Lineberger, W. C. *J. Chem. Phys.* **1990**, *93*, 6987.
(29) Rienstra-Kiracofe, J. C.; Tschumper, G. S.; Schaefer, H. F.; Nandi, S.; Ellison, G. B. *Chem. Rev.* **2002**, *102*, 231.
(30) Andersen, T.; Haugen, H. K.; Hotop, H. *J. Phys. Chem. Ref. Data* **1999**, *28*, 1511.
(31) Cooper, J.; Zare, R. N. *J. Chem. Phys.* **1968**, *48*, 942.
(32) MOLPRO is a package of ab initio programs written by Werner, H.-J. and Knowles, P. J. with contributions from Almlof, J.; Amos, R. D.; Bernhardsson, A.; Berning, A.; Celani, P.; Cooper, D. L.; Deegan, M. J. O.; Dobbyn, A. J.; Eckert, F.; Elbert, S. T.; Hampel, C.; Hetzer, G.; Korona, T.; Lindh, R.; Lloyd, A. W.; Mcnicholas, S. J.; Manby, F. R.; Meyer, W.; Mura, M. E.; Nicklass, A.; Palmieri, P.; Peterson, K. A.; Pitzer, R. M.; Pulay, P.; Rauhut, G.; Schutz, M.; Stoll, H.; Stone, A. J.; Tarroni, R.; Taylor, P. R.; Thorsteinsson, T.
(33) Raghavachari, K.; Trucks, G. W.; Pople, J. A.; Headgordon, M. *Chem. Phys. Lett.* **1989**, *157*, 479.
(34) Hampel, C.; Peterson, K. A.; Werner, H. J. *Chem. Phys. Lett.* **1992**, *190*, 1.
(35) Knowles, P. J.; Hampel, C.; Werner, H. J. *J. Chem. Phys.* **1993**, *99*, 5219.
(36) Watts, J. D.; Gauss, J.; Bartlett, R. J. *J. Chem. Phys.* **1993**, *98*, 8718.
(37) Werner, H. J.; Knowles, P. J. *J. Chem. Phys.* **1988**, *89*, 5803.
(38) Knowles, P. J.; Werner, H. J. *Chem. Phys. Lett.* **1988**, *145*, 514.
(39) Andrae, D.; Haussermann, U.; Dolg, M.; Stoll, H.; Preuss, H. *Theor. Chim. Acta* **1990**, *77*, 123.
(40) Bagatur'yants, A. A.; Safonov, A. A.; Stoll, H.; Werner, H. J. *J. Chem. Phys.* **1998**, *109*, 3096.
(41) Dunning, T. H. *J. Chem. Phys.* **1989**, *90*, 1007.
(42) Kendall, R. A.; Dunning, T. H.; Harrison, R. J. *J. Chem. Phys.* **1992**, *96*, 6796.
(43) Woon, D. E.; Dunning, T. H. *J. Chem. Phys.* **1993**, *98*, 1358.
(44) Obrien, L. C.; Kubicek, R. L.; Wall, S. J.; Koch, D. E.; Friend, R. J.; Brazier, C. R. *J. Mol. Spectrosc.* **1996**, *180*, 365.
(45) Obrien, L. C.; Wall, S. J.; Sieber, M. K. *J. Mol. Spectrosc.* **1997**, *183*, 57.
(46) Steimle, T.; Namiki, K.; Saito, S. *J. Chem. Phys.* **1997**, *107*, 6109.
(47) Steimle, T.; Tanimoto, M.; Namiki, K.; Saito, S. *J. Chem. Phys.* **1998**, *108*, 7616.
(48) The electron binding energy is the difference between the photon energy (3.408 eV) and the photoelectron kinetic energy.
(49) Ervin, K. M. *PESCAL, Fortran program*, 2003.
(50) Nakajima, A.; Taguwa, T.; Nakao, K.; Hoshino, K.; Iwata, S.; Kaya, K. *Surf. Rev. Lett.* **1996**, *3*, 417.
(51) Gilles, M. K.; Polak, M. L.; Lineberger, W. C. *J. Chem. Phys.* **1992**, *96*, 8012.
(52) Miller, C. E.; Cohen, E. A. *J. Chem. Phys.* **2001**, *115*, 6459.
(53) McKellar, A. R. W. *J. Mol. Spectrosc.* **1981**, *86*, 43.

(54) Burkholder, J. B.; Hammer, P. D.; Howard, C. J.; McKellar, A. R. W. *J. Mol. Spectrosc.* **1986**, *118*, 471.

(55) Burkholder, J. B.; Hammer, P. D.; Howard, C. J.; Maki, A. G.; Thompson, G.; Chackerian, C. *J. Mol. Spectrosc.* **1987**, *124*, 139.

(56) Tamassia, F.; Brown, J. M.; Evenson, K. M. *J. Chem. Phys.* **1999**, *110*, 7273.

(57) Howie, W. H.; Lane, I. C.; Newman, S. M.; Johnson, D. A.; Orr-Ewing, A. J. *Phys. Chem. Chem. Phys.* **1999**, *1*, 3079.

(58) Tamassia, F.; Brown, J. M.; Saito, S. *J. Chem. Phys.* **2000**, *112*, 5523.

(59) Drouin, B. J.; Miller, C. E.; Muller, H. S. P.; Cohen, E. A. *J. Mol. Spectrosc.* **2001**, *205*, 128.

(60) Tamassia, F.; Kermode, S. M.; Brown, J. M. *J. Mol. Spectrosc.* **2001**, *205*, 92.

(61) Drouin, B. J.; Miller, C. E.; Cohen, E. A.; Wagner, G.; Birk, M. *J. Mol. Spectrosc.* **2001**, *207*, 4.

(62) David, F.; Douay, M.; Lefebvre, Y. *J. Mol. Spectrosc.* **1985**, *112*, 115.

(63) O'Brien, L. C.; Wall, S. J.; Henry, G. L. *J. Mol. Spectrosc.* **1998**, *191*, 218.

(64) Thompsen, J. M.; Ziurys, L. M. *Chem. Phys. Lett.* **2001**, *344*, 75.

(65) Pitzer, K. S. *Acc. Chem. Res.* **1979**, *12*, 272.

(66) Pyykko, P.; Desclaux, J. P. *Acc. Chem. Res.* **1979**, *12*, 276.

(67) Pyykko, P. *Chem. Rev.* **1988**, *88*, 563.

(68) Polak, M. L.; Gilles, M. K.; Ho, J.; Lineberger, W. C. *J. Phys. Chem.* **1991**, *95*, 3460.

(69) Andrews, D. H.; Gianola, A. J.; Lineberger, W. C. *J. Chem. Phys.* **2002**, *117*, 4074.

(70) Langhoff, S. R.; Bauschlicher, C. W. *Chem. Phys. Lett.* **1986**, *124*, 241.

(71) Bauschlicher, C. W.; Partridge, H.; Langhoff, S. R. *Chem. Phys.* **1990**, *148*, 57.

(72) Allison, J. N.; Goddard, W. A. *J. Chem. Phys.* **1982**, *77*, 4259.

(73) Bagus, P. S.; Nelin, C. J.; Bauschlicher, C. W. *J. Chem. Phys.* **1983**, *79*, 2975.

(74) Breyer, F.; Frey, P.; Hotop, H. *Z. Phys. A* **1981**, *300*, 7.

(75) Schulz, P. A.; Mead, R. D.; Lineberger, W. C. *Phys. Rev. A* **1983**, *27*, 2229.

(76) Walker, T. E. H.; Waber, J. T. *J. Phys. B* **1974**, *7*, 674.

(77) Reed, K. J.; Zimmerman, A. H.; Andersen, H. C.; Brauman, J. I. *J. Chem. Phys.* **1976**, *64*, 1368.

(78) Lefebvre-Brion, H.; Field, R. W. *Perturbations in the spectra of diatomic molecules*; Academic Press: Orlando, 1986.

(79) Shepler, B. C.; Peterson, K. A. *J. Phys. Chem. A* **2003**, *107*, 1783.

(80) Branscomb, L. M.; Smith, S. J.; Tisone, G. *J. Chem. Phys.* **1965**, *43*, 2906.

(81) Hotop, H.; Lineberger, W. C. *J. Chem. Phys.* **1973**, *58*, 2379.

(82) Alternatively, second-order spin−orbit coupling between $^2\Pi_{1/2}$ and $^2\Sigma^+_{1/2}$AuO could lead to the intensity disparity between the two spin−orbit states. However, spin−orbit coupling calculations indicate that the mixing of the two neutral states is an order less than that of the two relevant anion states.